A Cartesian Grid Method for Compressible Inviscid Flows

M. Asif Farooq*, B. Müller
Department of Energy and Process Engineering, Faculty of Engineering Science
The Norwegian University of Science and Technology
e–mail: asif.m.farooq@ntnu.no, bernhard.muller@ntnu.no

Summary The Cartesian grid method has been investigated for the 2D compressible Euler equations. We impose wall boundary conditions by a simplified ghost point treatment for compressible inviscid flows with immersed boundaries. In the simplified ghost point treatment we assume the solid boundary lie in the middle between two grid points in the y direction. Symmetry conditions are used to determine density, pressure, wall tangential, and wall normal velocity components at the ghost points. A first order node-centered finite volume formulation has been used to calculate compressible flows. The order of this formulation is increased by employing MUSCL with the minmod limiter. The code is tested for external flows over a circular arc airfoil. We compare our results for the simplified ghost point treatment with a standard body-fitted grid method. We obtain similar results for the Cartesian grid method as for the standard body-fitted grid method for external flows.

Introduction

The Cartesian grid method has recently become one of the widely used methods in CFD [1, 2, 3, 4, 5, 6, 7, 8, 9]. Since solid boundaries are immersed in a Cartesian grid method with constant grid spacings, the Cartesian grid method is also called immersed boundary method, in particular in application to the incompressible Navier-Stokes equations. The popularity of the Cartesian grid method is due to its simplicity, faster grid generation, simpler programming, lower storage requirements, lower operation count, and easier post processing compared to body fitted structured and unstructured grid methods. The Cartesian grid method is also advantageous in constructing higher order methods. Problems occur at the boundary, when this method is applied to complex domains [10]. When the Cartesian grid method is applied at curved boundaries the cells at the boundaries are not rectangular and these cut-cells create problems for the scheme to be implemented [11]. The time step restriction problem caused by small cut-cells can be solved by merging those cut-cells with neighboring cells [7].

Cut cells are avoided altogether by ghost point treatment at the boundary. In this method symmetry conditions with respect to the boundary are imposed at ghost points in the solid adjacent to the boundary [12]. However, conservativity is lost in this process. Nevertheless, the simplicity of the ghost point treatment has motivated us to use that approach instead of the more complicated cut-cells.

Often the effect of solid boundaries cutting a Cartesian grid has been modelled by a force term in the incompressible momentum equations [13]. Since this approach is not so practical for compressible flow due to the sensitive coupling of all flow variables, it has not been used for compressible flow simulation except for [14, 2]. Instead, the effect of the tangency or slip condition at solid boundaries for inviscid compressible flow is used in the Cartesian grid method to determine the flow variables in ghost cells or at ghost points near solid boundaries [15, 16, 17, 12, 18, 19]. In the ghost point treatment we divide our domain into three types of points: fluid, ghost and solid points. For first and second order schemes the methods require one and two ghost points, respectively. Solid and ghost points are flagged inactive.

In this paper we employ a simplified ghost point treatment for the 2D compressible Euler equations. In the simplified ghost point treatment we assume the solid boundary lie in the middle

between two grid points in the y direction. Symmetry conditions are used to determine density, pressure, wall tangential, and wall normal velocity components at the ghost points. We employ the local Lax-Friedrichs (lLF) method for the spatial discretization. To increase the accuracy we apply the MUSCL approach with the minmod limiter. For time integration we use the first order explicit Euler method for spatially first order method and the third order TVD Runge-Kutta (RK3) method with the more accurate MUSCL approach. As a test case, we consider supersonic external over a circular arc airfoil and solve the 2D compressible Euler equations by time stepping for the steady state.

The paper is organized as follows. First we present the governing equations, i.e. the 2D compressible Euler equations then we outline the boundary conditions and explain the ghost point treatment at the embedded boundary. We present the discretization method, results and discussion and give conclusions.

Compressible Euler Equations

The 2D compressible Euler equations serve as a model for a 2D nonlinear hyperbolic system. In conservative form the 2D compressible Euler equations read

$$\frac{\partial U}{\partial t} + \frac{\partial F}{\partial x} + \frac{\partial G}{\partial y} = 0, \tag{1}$$

where

$$U = \begin{bmatrix} \rho \\ \rho u \\ \rho v \\ \rho E \end{bmatrix}, F = \begin{bmatrix} \rho u \\ \rho u^2 + p \\ \rho uv \\ (\rho E + p)u \end{bmatrix}, G = \begin{bmatrix} \rho v \\ \rho uv \\ \rho v^2 + p \\ (\rho E + p)v \end{bmatrix}, \tag{2}$$

with ρ , u, v, E, and p are density, velocity components in x-and y-directions, total energy per unit mass and pressure, respectively.

For perfect gas we have the following relation

$$p = (\gamma - 1)(\rho E - \frac{1}{2}\rho(u^2 + v^2)), \tag{3}$$

where γ is the ratio of specific heats. We consider γ = 1.4 for air.

Approximation of Boundary Conditions

Boundary Conditions for External Flow

The inflow boundary conditions for supersonic flow at $x = 0$ are imposed as

$$U_{1,j}(t) = U_\infty, \tag{4}$$

where U_∞ is the vector of the conservative variables for uniform flow in the $x-$ direction. The flow variables at the outlet $x = L_1$ are approximated as

$$U_{I,j}(t) = U_{I-1,j}(t), \tag{5}$$

i.e. by constant extrapolation. This approximation implies that the upwind finite volume method is used to determine the numerical fluxes $F_{I-\frac{1}{2},j}$.

The symmetry boundary conditions at $y = 0$ are implemented by considering an extra line below $y = 0$. There we use

$$U_{i,1}(t) = diag(1, 1, -1, 1)U_{i,3}(t). \tag{6}$$

The boundary conditions at $y = L_2$ are treated as

$$U_{i,J}(t) = U_{i,J-1}(t). \tag{7}$$

Ghost Point Treatment at Embedded Boundary

Simplified Ghost Point Treatment for Two Dimensional Embedded Boundary

In Fig. 1(a) we show the flagging strategy. We flag the ghost and solid points by assigning them 0 and -1 values. The fluid points are assigned values equal to 1. In Fig. 1(b) we show a simplified ghost point treatment at the solid boundary. A ghost point is denoted by G. In the simplified ghost point treatment we consider the fluid point F on the vertical grid line through G adjacent to the boundary as the mirror point. Then, we assume the boundary is in the middle between ghost and fluid points. The density ρ, pressure p, and the tangential velocity component at the ghost point are symmetric with respect to the solid boundary and therefore directly determined by their values at F. The normal velocity component u_n at the ghost point is anti-symmetric and thus gets the negative value of u_n at F. The mathematical description of this strategy is given as

$$\rho_G = \rho_F, p_G = p_F, u_G = u_F - 2(n_1u_F + n_2v_F)n_1, v_G = v_F - 2(n_1u_F + n_2v_F)n_2, \tag{8}$$

where n_1 and n_2 are the x-and y-components of the outer unit normal **n** of the boundary.

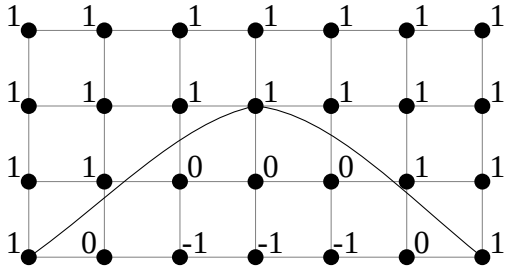

(a) Flagging strategy for fluid (1), ghost (0) and solid points (-1).

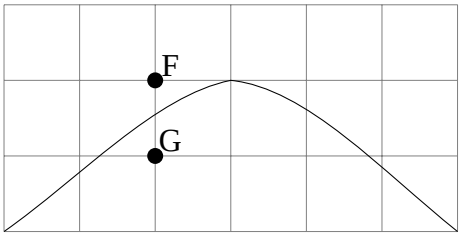

(b) Simplified ghost point treatment over a circular arc airfoil.

Figure 1: Ghost point treatment.

Discretization of the Euler Equations

Spatial Discretization

We assume a rectangular domain [0 L_1] $\times$ [0 L_2] and a $(I + 1) \times (J + 1)$ Cartesian grid with equidistant grid spacing $\Delta x = L_1/I$ and $\Delta y = L_2/J$. The Cartesian coordinates of the grid points (i, j) are (x_i, y_j), where $x_i = i\Delta x$, $i = 0, 1, ..., I$, and $y_j = j\Delta y$, $j = 0, 1, ..., J$.

The node-centered finite volume method yields the following semi-discretization of the 2D compressible Euler equations (1)

$$\frac{\mathrm{d}U_{i,j}}{\mathrm{d}t} = -\frac{F_{i+\frac{1}{2},j} - F_{i-\frac{1}{2},j}}{\Delta x} - \frac{G_{i,j+\frac{1}{2}} - G_{i,j-\frac{1}{2}}}{\Delta y}. \tag{9}$$

Where $U_{i,j}$ is the approximation of the average of U in the cell $\Omega_{i,j} = [x_i - \frac{\Delta x}{2}, x_i + \frac{\Delta x}{2}] \times [y_j - \frac{\Delta y}{2}, y_j + \frac{\Delta y}{2}]$, i.e.

$$U_{i,j} \approx \frac{1}{\Delta x.\Delta y} \int_{\Omega_{i,j}} U(x,y,t)dxdy. \tag{10}$$

If we interpret (9) as a conservative finite difference method, $U_{i,j}$ is an approximation of the exact solution $U(x_i, y_j, t)$. $F_{i+\frac{1}{2},j}$ and $G_{i,j+\frac{1}{2}}$ are numerical fluxes for the 2D compressible Euler equations at the cell faces ($i + \frac{1}{2}$, j) and (i, $j + \frac{1}{2}$), respectively. The vector of the conservative variables U and the flux vectors F and G are defined in (2). The numerical fluxes of the local Lax-Friedrichs (lLF) method are defined as follows

$$F^{lLF}_{i+\frac{1}{2},j} = \frac{1}{2}\left[F(U_{i,j}) + F(U_{i+1,j}) - max(|u_{i+1,j}| + c_{i+1,j}, |u_{i,j}| + c_{i,j})(U_{i+1,j} - U_{i,j})\right], \tag{11}$$

$$G^{lLF}_{i,j+\frac{1}{2}} = \frac{1}{2}\left[G(U_{i,j}) + G(U_{i,j+1}) - max(|u_{i,j+1}| + c_{i,j+1}, |u_{i,j}| + c_{i,j})(U_{i,j+1} - U_{i,j})\right]. \tag{12}$$

In equations (11) and (12), c is the speed of sound. The CFL number for the 2D compressible Euler equations is defined as $CFL = \Delta t \underset{i,j}{max}\left(\frac{sp(A_1(U_{i,j}))}{\Delta x} + \frac{sp(A_2(U_{i,j}))}{\Delta y}\right)$, where $sp(A_1(U_{i,j}))$ and $sp(A_2(U_{i,j}))$ are the spectral radii of the Jacobian matrices $A_1 = \frac{\partial F}{\partial x}$ and $A_2 = \frac{\partial G}{\partial y}$, respectively. We choose $CFL = 0.5$ for the results of the 2D compressible Euler equations presented below. In (11) we replace $U_{i,j}$ by $U^L_{i+\frac{1}{2},j}$ and $U_{i+1,j}$ by $U^R_{i+\frac{1}{2},j}$ using the MUSCL approach with the minmod limiter to obtain second order accuracy except for extrema without undesired oscillations. The extrapolated variables are defined as

$$U^L_{i+\frac{1}{2},j} = U_{i,j} + \frac{1}{2} minmod(U_{i,j} - U_{i-1,j}, U_{i+1,j} - U_{i,j}), \tag{13}$$

$$U^R_{i+\frac{1}{2},j} = U_{i+1,j} - \frac{1}{2} minmod(U_{i+2,j} - U_{i+1,j}, U_{i+1,j} - U_{i,j}). \tag{14}$$

where

$$minmod(a,b) = \begin{cases} a & if\,|a| \le |b| \quad and \quad ab > 0 \\ b & if\,|b| < |a| \quad and \quad ab > 0 \\ 0 & if ab \le 0 \end{cases} \tag{15}$$
$$= sign(a) max\left\{0, min\left\{|a|, sign(a)b\right\}\right\}$$

is the minmod limiter. The MUSCL approach is applied similarly to the numerical fluxes $G_{i,j+\frac{1}{2}}$ in (12).

Temporal Discretization

For time integration we use the explicit Euler method and the total variation diminishing third order Runge-Kutta (TVD RK3) method. The explicit Euler method is defined as follows

$$U^{n+1} = U^n + \Delta t \mathbf{Res}(U^n), \tag{16}$$

where $\mathbf{Res}(U^n)$ at (i,j) is the residual, i.e. the right hand side of (9). The TVD RK3 method is given as

$$\begin{aligned} U^{(1)} &= U^n + \Delta t \mathbf{Res}(U^n), \\ U^{(2)} &= \frac{3}{4}U^n + \frac{1}{4}U^{(1)} + \frac{1}{4}\Delta t \mathbf{Res}(U^{(1)}), \\ U^{(n+1)} &= \frac{1}{3}U^n + \frac{2}{3}U^{(2)} + \frac{2}{3}\Delta t \mathbf{Res}(U^{(2)}). \end{aligned} \tag{17}$$

Results

Two Dimensional Compressible Euler Equations

We verify our 2D code of the Cartesian grid method for external flow over a circular arc airfoil. For the spatial discretization we use the local Lax-Friedrichs (lLF) method, and to increase the order of our method we employ the MUSCL scheme with the minmod limiter. For time integration we use the first order explicit Euler and third order TVD Runge-Kutta (RK3) methods. We use the CFL number 0.5 and 81 $\times$ 81 grid points to calculate the density ρ, velocities u and v, and pressure p.

External Flow Over a Circular Arc Airfoil

A supersonic flow moves from left to right and hits a circular arc airfoil of which we only consider the upper half. We consider the length of domain in $x-$and $y-$directions is $L_1 = 2m$ and $L_2 = 1m$ respectively. The height of the half circular arc airfoil is 10 $\%$ of its chord length which is assumed to be 1m. The supersonic upstream flow conditions are given as

$$M_\infty = 2, p_\infty = 10^5 Pa, \rho_\infty = 1.2 kg/m^3 \tag{18}$$

Results for the Cartesian Grid Method

In Fig. 2(a) and Fig. 2(b) we present Mach number and density contours for external flow at $M_\infty = 2$ over the circular arc airfoil. We compute only the flow over the upper half with a height of 10 $\%$ chord. The supersonic flow is moving from left to right and hits the leading edge of the circular arc airfoil. A shock wave is produced at the leading edge. Near the trailing edge another shock wave turns the flow back in the $x-$direction.

In Fig. 3(a) and Fig. 3(b) we present contours of the velocity components u and v.

Fig. 4(a) shows the behavior of the pressure for external flow over a circular arc airfoil.

In Fig. 4(b) the l_2-norm of the density change, which is equivalent to the density residual, indicated that the density is becoming stationary after around $n = 2500$ iterations. We have not yet explored the kink in the convergence curve leading to slower convergence.

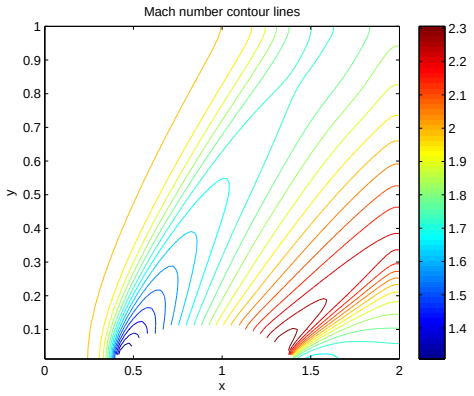

(a) Mach number contours for supersonic external flow over a circular arc airfoil.

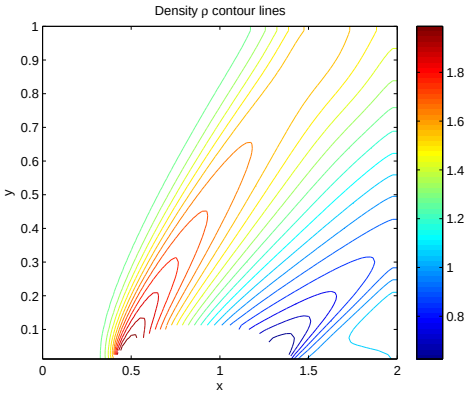

(b) Density contours for supersonic external flow over a circular arc airfoil.

Figure 2: Left: Mach number contours for first order method. Right: Density contours for first order method .

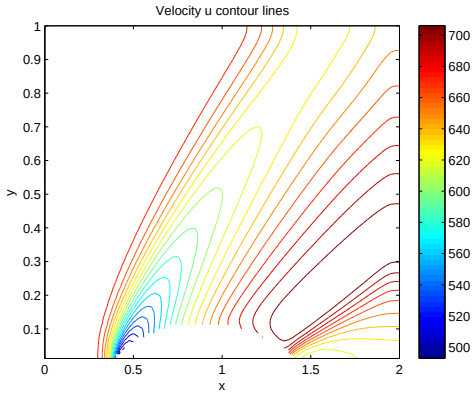

(a) Velocity u component contours for supersonic external flow over a circular arc airfoil.

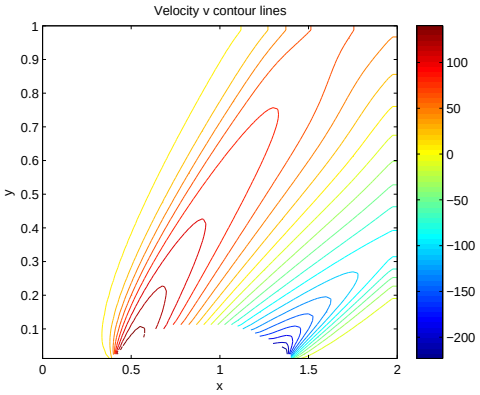

(b) Velocity v component contours for supersonic external flow over a circular arc airfoil.

Figure 3: Left: Velocity component u contours for first order method. Right: Velocity v component contours for first order method.

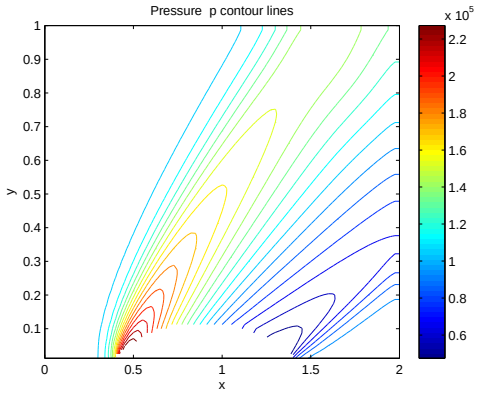

(a) Pressure contours for supersonic external flow over a circular arc airfoil.

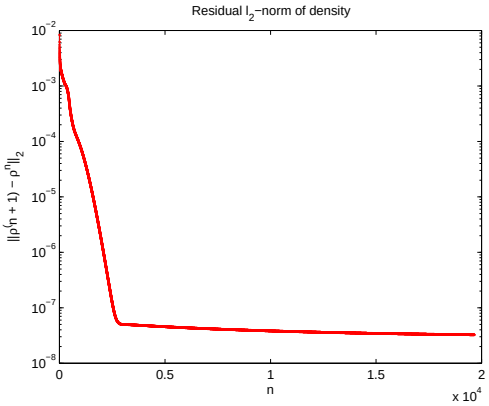

(b) Residual l_2-norm of density for supersonic flow over a circular arc airfoil.

Figure 4: Left: Pressure contours for first order method. Right: Residual l_2-norm of density for first order method.

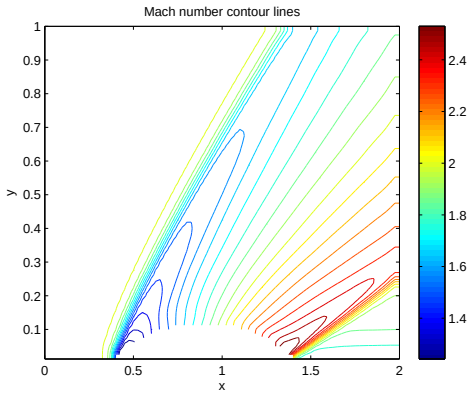

(a) Mach number contours for supersonic external flow over a circular arc airfoil.

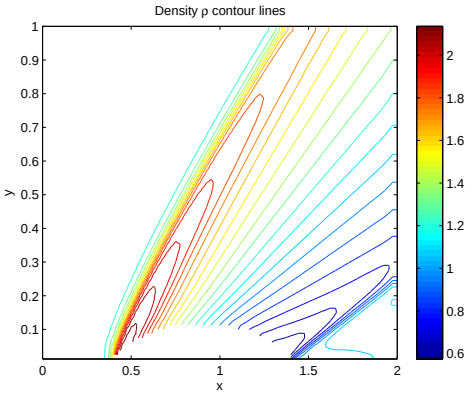

(b) Density contours for supersonic external flow over a circular arc airfoil.

Figure 5: Left: Mach number contours for MUSCL with the minmod limiter. Right: Density contours for MUSCL with the minmod limiter.

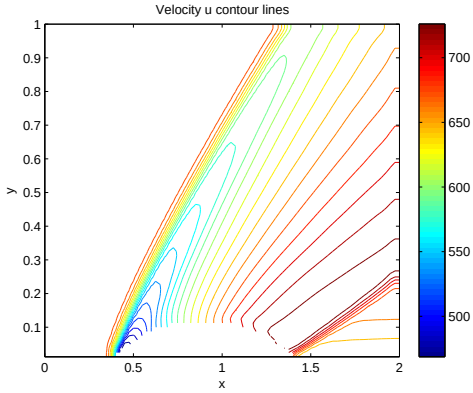

(a) Velocity component u contours for supersonic external flow over a circular arc airfoil.

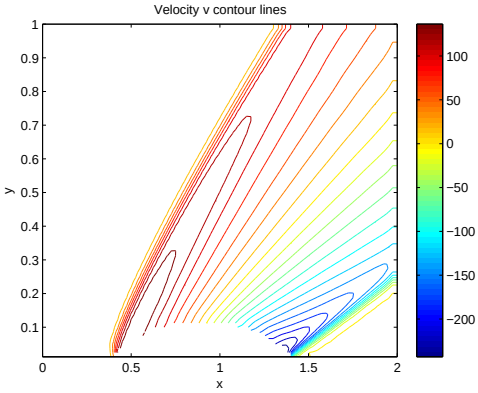

(b) Velocity component v contours for supersonic external flow over a circular arc airfoil.

Figure 6: Left: Velocity component u contours for MUSCL with the minmod limiter. Right: Velocity v component for MUSCL with the minmod limiter.

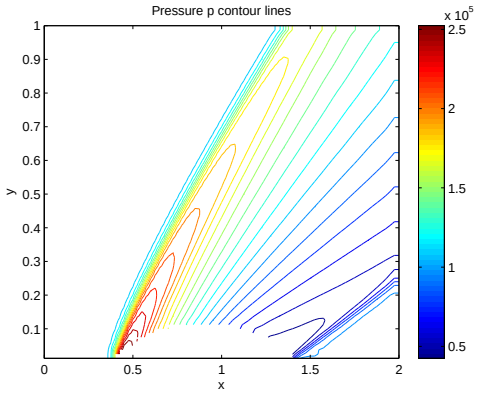

(a) Pressure contours for supersonic external flow over a circular arc airfoil.

Figure 7: Pressure contours for MUSCL with the minmod limiter.

Now we turn to the results obtained with the higher order method. We use the local Lax-Friedrichs method for spatial discretization with MUSCL and minmod limiter and TVD RK3 method for time integration. We obtain sharp shock waves at the leading and trailing edges , cf. Fig. 5(a) and Fig. 5(b) for Mach number and density contours. Whereas the first order results in Figs. 2, 3, 4(a) yield a detached shock like for blunt body flow, the second order MUSCL results (first order at extrema) indicate an attached oblique shock in agreement with the corresponding body-fitted grid results, cf. below.

In Fig. 6(a) and Fig. 6(b) we present results over the circular arc airfoil for the velocity components u and v for higher order method for external flows. The shock wave at the leading and trailing edges is sharper than for the first order method, cf. Fig. 3.

Also the pressure contours with the higher order method in Fig. 7(a) indicate sharper leading and trailing edge shocks than the first order method, cf. Fig. 4(a).

Results for the Standard Body-Fitted Grid Method

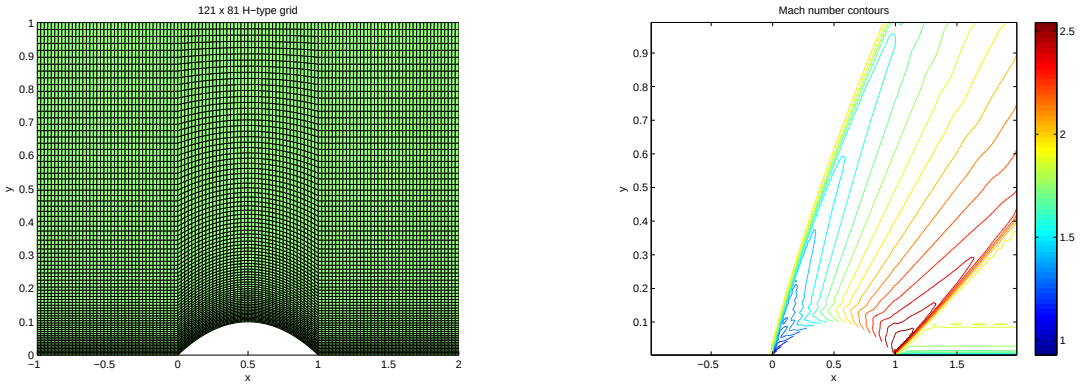

(a) Standard body-fitted grid.

(b) Mach number contours for supersonic external flow over a circular arc airfoil.

Figure 8: Left: Standard body-fitted grid of a circular arc airfoil. Right: Mach number contours for standard body-fitted method.

The grid spacing in the $x-$direction is the same as for the Cartesian grid method, i.e. $\Delta x = \frac{1}{40}$. The grid points are clustered towards $y = 0$ and the circular arc airfoil ($\Delta y_{min} = 0.0037$ at $y = 0$ and $\Delta y_{max} = 0.0208$ at $y = 1$). The body-fitted grid for the the domain has 121×81 grid points (cf. Fig. 8(a)), because the left and right boundaries are one chord length away from the leading and trailing edges respectively.

The cell-centered finite volume method with Roe's approximate Riemann solver is used, which is less diffusive than the local Lax-Friedrichs method. The MUSCL approach is applied to the primitve variables, not in the conservative variables as in (13) and (14). While the minmod limiter is used for density and pressure, the less diffusive van Albada limiter is employed for the velocity components. Harten's entropy fix is employed to enforce the entropy condition [20, 21].

The contours for Mach number, density, velocities components u and v and pressure contours in Fig. 8(b), Fig. 9 and Fig. 10 for a same supersonic flow over the circular arc airfoil show that the standard-body fitted grid method yields sharper shocks at the leading and trailing edges. Note that density, velocities components u and v and pressure are non-dimensionalized with respect to reference density ρ_∞, velocity u_∞ and pressure $\rho_\infty u_\infty^2$, respectively. But otherwise, there is

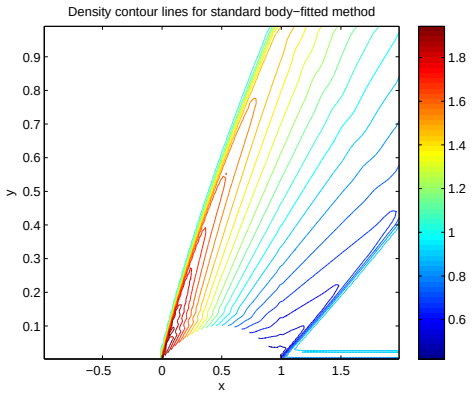

(a) Density contours for supersonic external flow over a circular arc airfoil.

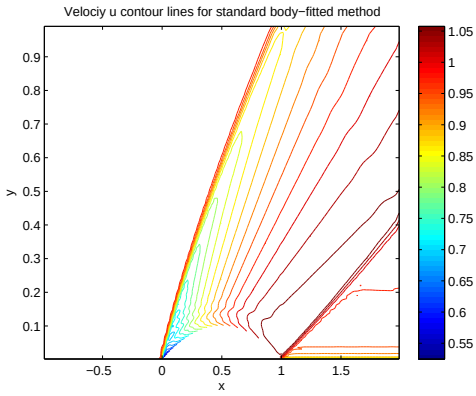

(b) Velocity component u contours for supersonic external flow over a circular arc airfoil.

Figure 9: Left: Density contours for standard body-fitted method. Right: Velocity component u contours for standard body-fitted method.

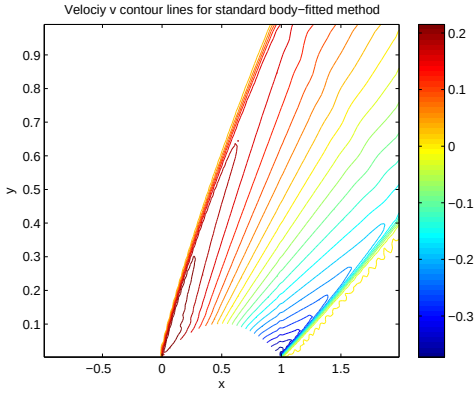

(a) Velocity component v contours for supersonic external flow over a circular arc airfoil.

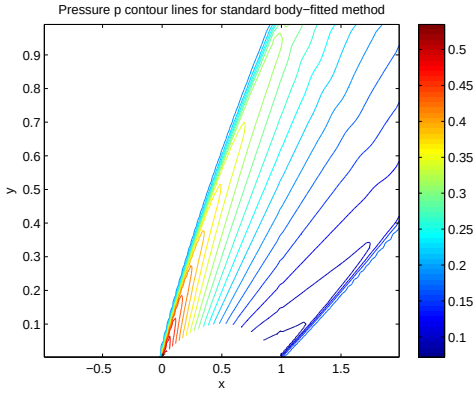

(b) Pressure contours for supersonic external flow over a circular arc airfoil.

Figure 10: Left: Velocity contours for standard body-fitted method. Right: Pressure contours for standard body-fitted method.

good qualitative agreement between the body-fitted results and the Cartesian grid method with MUSCL, cf. Fig. 5, Fig. 6 and Fig. 7(a). Note that the wiggles behind the leading edge shock for Mach number M, density ρ and velocity u are not present for the Cartesian grid method.

Conclusions

We investigated the Cartesian grid method for the 2D compressible Euler equations. We used the first order local Lax-Friedrichs method for spatial discretization and increased the accuracy by MUSCL with the minmod limiter. For time integration we used the first order explicit Euler method and the third order TVD RK3 method. At the immersed solid boundary we employed a simplified ghost point treatment in which the fluid point F is chosed on the vertical grid line through G adjacent to the boundary as the mirror point. We tested the 2D code for supersonic external flow over a circular arc airfoil. The comparison between the Cartesian grid method and the standard body-fitted grid method indicated good qualitative agreement.

Acknowledgement

The current research has been funded by the Higher Education Commission (HEC) of Pakistan.

References

[1] Almgren, A. S., Bell, J. B., Colella, P. & Marthaler, T. A Cartesian grid projection method for the incompressible Euler equations in complex geometries. *SIAM Journal on Scientific Computing* **18**, 1289–1309 (1997).

[2] Palma, P. D., de Tullio, M. D., Pascazio, G. & Napolitano, M. An immersed-boundary method for compressible viscous flows. *Computers & Fluids* **35**, 693–702 (2006).

[3] Marshall, D. D. & Ruffin, S. M. . A new inviscid wall boundary condition treatment for boundary Cartesian grid method. *AIAA 2004-0583 42nd AIAA Aerospace Sciences Meeting and Exhibit, Reno, Nevada* (2004).

[4] Udaykumar, H. S., Krishnann, S. & Marella, S. V. Adaptively refined parallelisded sharp interface Cartesian grid method for three dimensional moving boundary problem. *International Journal of Computational Fluid Dynamics* **23**, 1–24 (2009).

[5] Uzgoren, E., Sim, J. & Shyy, W. Marker based 3-D adapitve Cartesian grid method for multiphase flow around irregular geometries. *Communications in Computational Physics* **5**, 1–41 (2009).

[6] Wang, Z., Fan, J. & Cen, K. Immersed boudnary method for the simulations of 2D viscous flow based on vorticity-velocity formulations. *Journal of Computational Physics* **228**, 1504–1520 (2009).

[7] Mittal, R. & Iaccarino, G. Immersed boundary methods. *Annual Review of Fluid Mechanics* **37**, 239–261 (2005).

[8] Kirshman, D. & Liu, F. Cartesian grid solution of the Euler equations using a gridless boundary condition treatment. *AIAA Paper 2003-3974* (2003).

[9] Peng, Y.-F., Mittal, R., Sau, A. & Hwang, R. R. Nested Cartesian grid method in incompressible viscous fluid flow. *Journal of Computational Physics* **229**, 7072–7101 (2010).

[10] Quirk, J. J. An alternative to unstructured grids for computing gas dynamic flows around arbitrarily complex two -dimensional bodies. *Computers & Fluids* **23**, 125–142 (1994).

[11] Ingram, D., Causon, D. & Mingham, C. Developments in Cartesian cut cell methods. *Mathematics and Computers in Simulation* **61**, 561572 (2003).

[12] Forrer, H. & Jeltsch, R. A higher-order boundary treatment for Cartesian-grid methods. *Journal of Computational Physics* **140**, 259–277 (1998).

[13] S.Peskin, C. Flow pattern around heart valves: A numerical method. *Journal of Computational Physics* **10**, 252–271 (1972).

[14] de Tullio, M. D., Palma, P. D. D., Iaccarino, G., Pascazio, G. & Napolitano, M. An immersed boundary method for compresible flows using local grid refinement. *Journal of Computational Physics* **225**, 2098–2117 (2007).

[15] Berger, M. J. & LeVeque, R. J. A rotated difference scheme for Cartesian grids in complex geometries. *AIAA Paper CP-91-1602* **CP-91-1602**, 1–9 (1991).

[16] Pember, R. B., Bell, J. B., Colella, P., Curtchfield, W. Y. & Welcome, M. L. An adaptive Cartesian grid method for unsteady compressible flow in irregular regions. *Journal of Computational Physics* **120**, 278–304 (1995).

[17] Coirier, W. J. & Powell, K. G. An accuracy assessment of Cartesian-mesh approaches for the Euler equations. *Journal of Computational Physics* **117**, 121–131 (1995).

[18] Colella, P., Graves, D. T., Keen, B. J. & Modiano, D. A Cartesian grid embedded boundary method for hyperbolic conservation laws. *Journal of Computational Physics* **211**, 347–366 (2006).

[19] Sjögreen, B. & Petersson, N. A. A Cartesian embedded boundary method for hyperbolic conservation laws. *Communications in Computational Physics* **2**, 1199 – 1219 (2007).

[20] Harten, A. High resolution schemes for hyperbolic conservation laws. *Journal of Computational Physics* **49**, 357–393 (1983).

[21] Müller, B. Upwind relaxation method for hyperbolic flow simulation. *Technical Report DLR-FB Göttingen, Germany*, 91–36 (1991).